IEEE Access
Multidisciplinary | Rapid Review | Open Access Journal

Received January 15, 2019, accepted January 29, 2019, date of publication February 1, 2019, date of current version February 20, 2019.

Digital Object Identifier 10.1109/ACCESS.2019.2896884

Design of Compact Filtering 180-Degree Hybrids With Arbitrary Power Division and Filtering Response

CHI-FENG CHEN, (Member, IEEE), JHONG-JHEN LI, GUO-YUN WANG, KAI-WEI ZHOU, AND RUEI-YI CHEN

Department of Electrical Engineering, Tunghai University, Taichung 40704, Taiwan

Corresponding author: Chi-Feng Chen (cfchen@thu.edu.tw)

This work was supported by the Ministry of Science and Technology, Taiwan, under Grant MOST 106-2221-E-029-001 and Grant MOST 107-2221-E-029-009.

ABSTRACT The design of filtering 180° hybrids with arbitrary power division and filtering response (filter order) is proposed in this paper. By integrating a 180° hybrid and bandpass filters into a single component, the overall circuit size can be reduced. The design theory based on the coupled resonator technique was detailed and validated experimentally through the fabrication of the third-order filtering 180° hybrid with a 0-dB power-dividing ratio and the second-order filtering 180° hybrid with a 6-dB power-dividing ratio. The power-dividing ratio can be arbitrarily determined through proper design of the coupling coefficients between the resonators. In addition, net-type resonators were selected to ensure compactness of the filtering 180° hybrids. The prototype sizes of the two example circuits were only approximately $0.25\lambda_g \times 0.12\lambda_g$ and $0.12\lambda_g \times 0.12\lambda_g$, demonstrating highly compact circuit sizes. Moreover, isolations better than 30 and 21 dB within the operating passbands for the two circuits were achieved.

INDEX TERMS 180-degree hybrids, arbitrary power division, bandpass filters (BPFs), microstrip.

I. INTRODUCTION

In radio frequency (RF) and microwave wireless communication systems, bandpass filters (BPFs) and hybrids (or couplers) are critical and essential components, which are used to select and divide or combine RF signals or power, respectively [1]. In recent years, integrating a hybrid and BPFs into a single device, namely a filtering hybrid, has become popular, because it can not only reduce the number of RF and microwave components but also save circuit area in various systems. In [2]–[10], the transformation of a 180° hybrid into a coupled resonator network has been investigated. Size reduction could be achieved because the λ/4 and 3λ/4 transmission line sections were replaced with coupling between resonators. Moreover, a filtering function could be obtained. In [11], a dual-band filtering quadrature (90°) hybrid was proposed. Power-dividing and filtering functions were achieved simultaneously by using two sets of coupled resonators. A dual-band filtering 90° hybrid based on the coupled resonator technique was investigated in [12]. The use of dual-mode stub- loaded resonators to fabricate a filtering 90° hybrid resulted in a compact structure. To enhance frequency selectivity, a 180° hybrid with an eighth-order bandpass response was developed in [13]. In [14], a collaborative design of a dual-band filtering 180° hybrid using shorted-stub loaded stepped-impedance resonators was presented. The electric and magnetic coupling coefficients for the two passbands can be determined by adjusting the structural parameters of an open coupled line and three shorted stubs. Moreover, several dual-band 180° hybrids have been proposed in [15]–[19] by using different design methods.

In addition, the hybrid coupler with arbitrary power division is required for certain applications. Accordingly, several approaches have been reported in [20]–[26]. In [20], a periodic stepped-impedance ring structure was proposed for implementing 180° hybrids with arbitrary power division. In [21], a miniaturized dual-band 180° hybrid with arbitrary power divisions was designed. Here, each λ/4 section of a traditional rat-race coupler was replaced with the proposed elementary two-port networks. In [22], branch-line

The associate editor coordinating the review of this manuscript and approving it for publication was Yingsong Li.

and rat-race couplers were designed using arbitrary power division ratios. A stepped-impedance section possessing two shunt open stubs was used for the designs. In [23], a dual transmission line comprising two parallel-connected high-impedance transmission lines with unequal electrical lengths were used to implement a 180° hybrid with an arbitrary power division ratio. In [24], a dual-band 180° hybrid based on a stepped-impedance double-sided parallel-strip line with arbitrary power divisions was studied. In [25], a 180° hybrid with negative group delay characteristics and an arbitrary power division ratio was developed. Furthermore, a design method for unequal power division filtering rat-race ring couplers was proposed in [26]. Two fifth-order filtering rat-race ring couplers with 3 and 10 dB power divisions were designed and implemented for demonstration.

To achieve both dividing and combining power and filtering functions, the traditional scheme is to cascade a 180° hybrid and two BPFs, as shown in Fig. 1(a). However, this leads to a large circuit area of the RF/microwave communication system. To miniaturize the circuit area, an effective design is to integrate the 180° hybrid and BPFs into a single component, as illustrated in Fig. 1(b). Although the 180° filtering hybrids reported in [2]–[10], [13], and [14] exhibit a high frequency selectivity property, these designs do not provide arbitrary power division. Moreover, the hybrid couplers reported in [20]–[25] have been designed to have an arbitrary power-dividing function, but such designs lack filtering characteristics. Thus, our research aimed to design compact filtering 180° hybrids with arbitrary power division and filtering response. A third-order filtering 180° hybrid with an output power-dividing ratio of 0 dB and a second-order filtering 180° hybrid with an output power-dividing ratio of 6 dB were designed, fabricated, and measured for demonstration. The measured results agreed well with the theoretical and simulated ones and thus verify the proposed theory and method.

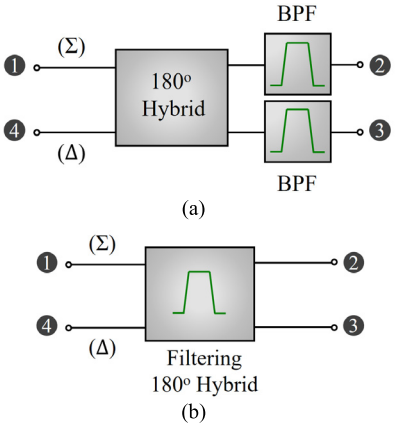

FIGURE 1. Block diagrams. (a) Cascade of a 180° hybrid and two BPFs and (b) filtering 180° hybrid.

The rest of this paper is organized as follows. Section II presents the design theory and procedures for the proposed filtering 180° hybrids in detail. In Section III, two design cases for the proposed filtering 180° hybrids with different specifications are provided. The experimental results are presented and are compared with the electromagnetic simulation results. Finally, Section IV presents the conclusion.

II. DESIGN THEORY

A 180° hybrid is a four-port network and can be considered as a combination of in-phase and out-of-phase power dividers [27]. The scattering parameters of a 180° hybrid with arbitrary power division can be expressed as follows:

$$[S] = \begin{bmatrix} 0 & \alpha & \beta & 0 \\ \alpha & 0 & 0 & -\beta \\ \beta & 0 & 0 & \alpha \\ 0 & -\beta & \alpha & 0 \end{bmatrix} \tag{1}$$

To satisfy power conservation, the condition of $\alpha^2 + \beta^2 = 1$ should be satisfied. Here, the output power-dividing ratio is defined as

$$P_{ratio} = 10log\frac{\alpha^2}{\beta^2}\,(\text{dB}) \tag{2}$$

In addition, a Chebyshev BPF can be designed using the coupled resonator technique. By calculating and extracting the desired coupling coefficients and external quality factors, the structural parameters of the BPF can be determined [28]. The typical coupling topology of an nth-order Chebyshev BPF is illustrated in Fig. 2(a), where each node denotes a resonator; $M_{i,j}$ represents the coupling coefficient between resonators i and j, and Q_e represents the external quality factor. The equivalent circuit of the nth-order Chebyshev BPF is illustrated in Fig. 2(b). Here, the coupling coefficient and external quality factor are defined as follows [28]:

$$M_{i,j} = \frac{L_{ij}}{\sqrt{L_i L_j}} \tag{3}$$

and

$$Q_e = \frac{\omega_0 L_1}{R_1} = \frac{\omega_0 L_n}{R_n} \tag{4}$$

where L_{ij} represents the mutual inductance between resonators i and j, and L, C, and R represent the inductance, capacitance, and resistance, respectively.

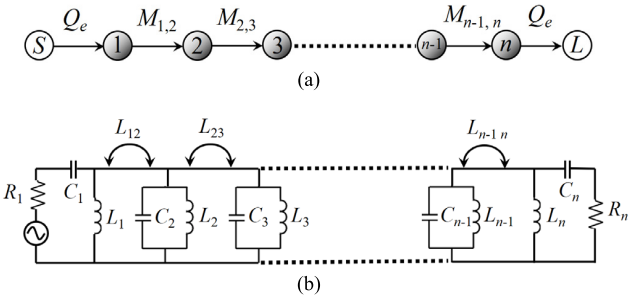

FIGURE 2. The nth-order Chebyshev BPF. (a) Coupling topology and (b) equivalent circuit.

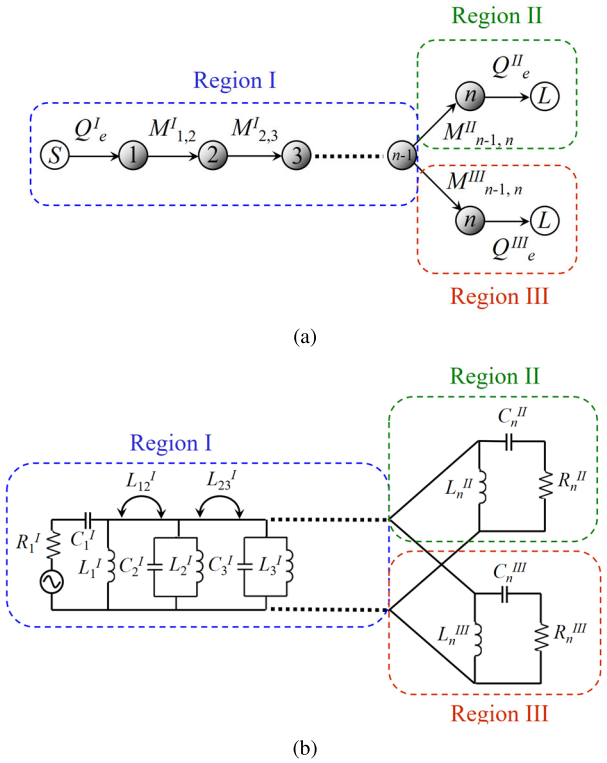

FIGURE 3. Filtering power divider. (a) Coupling topology and (b) equivalent circuit.

Fig. 3(a) illustrates the coupling topology of an nth-order filtering power divider. Power splitting was performed at the resonator $n-1$ in this illustrated topology. The equivalent circuit of the filtering power divider is provided in Fig. 3(b). To realize an identical filtering response with an nth-order Chebyshev BPF, the relationships between the circuit parameters of Fig. 2 and Fig. 3 can be found as follows:

Region I:

$$\begin{aligned} R_1^I &= R_1 \\ L_i^I &= L_i \\ C_i^I &= C_i \\ L_{ij}^I &= L_{ij} \end{aligned} \tag{5}$$

Region II:

$$\begin{aligned} R_n^{II} &= \frac{\alpha^2}{\alpha^2+\beta^2} R_n \\ L_n^{II} &= \frac{\alpha^2}{\alpha^2+\beta^2} L_n \\ C_n^{II} &= \frac{\alpha^2+\beta^2}{\alpha^2} C_n \\ L_{n-1,n}^{II} &= \frac{\alpha^2}{\alpha^2+\beta^2} L_{n-1,n} \end{aligned} \tag{6}$$

Region III:

$$\begin{aligned} R_n^{III} &= \frac{\beta^2}{\alpha^2+\beta^2} R_n \\ L_n^{III} &= \frac{\beta^2}{\alpha^2+\beta^2} L_n \\ C_n^{III} &= \frac{\alpha^2+\beta^2}{\beta^2} C_n \\ L_{n-1,n}^{III} &= \frac{\beta^2}{\alpha^2+\beta^2} L_{n-1,n} \end{aligned} \tag{7}$$

According to (3) and (4), the relationships of the coupling coefficients and external quality factors between an nth-order Chebyshev BPF and an nth-order filtering power divider can be derived as follows:

$$\begin{aligned} M_{i,i+1}^I &= M_{i,i+1},\ i = 1 \text{ to } n-2 \\ M_{n-1,n}^{II} &= \alpha M_{n-1,n} \\ M_{n-1,n}^{III} &= \beta M_{n-1,n} \end{aligned} \tag{8}$$

and

$$Q_e^I = Q_e^{II} = Q_e^{III} = Q_e \tag{9}$$

In summary, once the specifications, including central frequency, bandwidth, filter order, passband ripple, and power-dividing ratio, are allotted, the required coupling coefficients, $M_{i,i+1}^I$, $M_{n-1,n}^{II}$, and $M_{n-1,n}^{III}$, and external quality factors, Q_e^I, Q_e^{II}, and Q_e^{III}, of a filtering power divider can then be calculated. Note that, the analysis above is based on magnetic couplings. If the couplings between resonators are electric couplings, the idea is also suitable for use.

The proposed coupling topology of a filtering 180° hybrid with nth-order Chebyshev bandpass response and arbitrary power division is presented in Fig. 4, where ports 1 and 4 are defined as the sum and difference ports, respectively. The structure was formed by in-phase and out-of-phase filtering power dividers. To achieve a 180° phase difference between the output ports of an out-of-phase filtering power divider, the coupling route marked with dashed line should be out-of-phase with the others; that is, the sign of the coupling coefficient is negative, which is opposite that of the other coupling coefficients. Here, the frequency selectivity can be arbitrarily determined by selecting different values of the filter order n. Moreover, a high filter order results in high selectivity. For example, the ideal frequency responses of a filtering 180° hybrid centered at 1 GHz with different values of power-dividing ratio (P_{ratio}), filter order (n), and fractional bandwidth (Δ) are presented in Fig. 5(a)–(d). We observed that a filtering response with arbitrary power division and filter order can be achieved. It should be noted that, since the proposed filtering 180° hybrid is designed by using the coupled resonator technique, which is based on narrowband

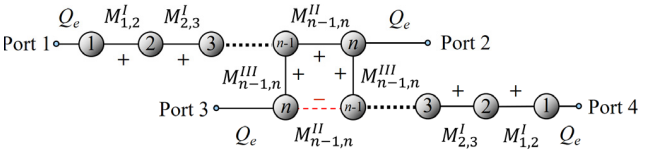

FIGURE 4. Proposed coupling topology of a filtering 180° hybrid.

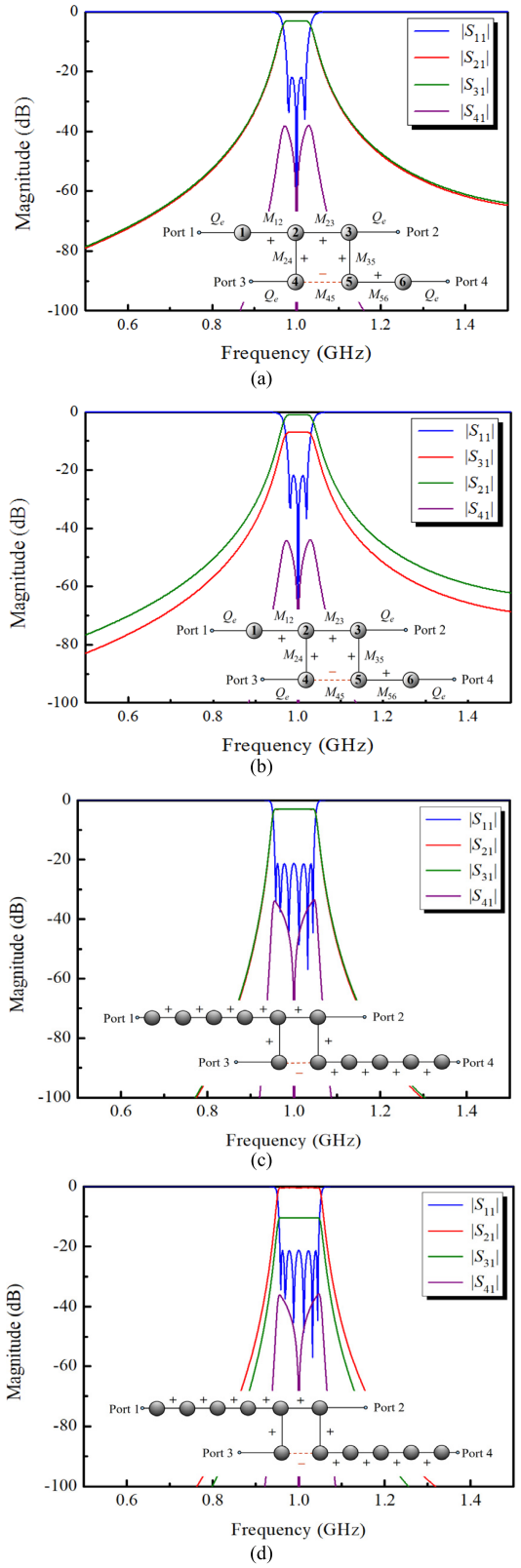

FIGURE 5. Responses of the filtering 180° hybrid. (0.04321 dB ripple level) (a) $P_{ratio} = 0$ dB, $n = 3$, and $\Delta = 5\%$; (b) $P_{ratio} = 6$ dB, $n = 3$, and $\Delta = 5\%$; (c) $P_{ratio} = 0$ dB, $n = 6$, and $\Delta = 10\%$; (d) $P_{ratio} = 10$ dB, $n = 6$, and $\Delta = 10\%$.

approximation, hence the proposed method and structure are applicable to the narrowband realization, i.e., $\Delta \leq 20\%$.

The design procedures of the proposed filtering 180° hybrid are summarized as follows.

Step 1) Prescribe the central frequency, bandwidth, filter order, passband ripple, and power-dividing ratio.

Step 2) Select the type of resonator. Note that the fundamental resonance frequency of all resonators should be designed to correspond to the central frequency of the hybrid.

Step 3) Calculate the theoretical values of coupling coefficients and external quality factors according to the specification.

Step 4) Extract coupling coefficients of coupled resonators and external quality factors of input–output (I/O) coupling structure.

Step 5) Determine the gap distance between adjacent resonators and physical parameters of the I/O coupling structure according to the theoretical values of coupling coefficients and I/O external quality factors.

Step 6) Perform an optimization procedure to acquire a specific passband performance level (if required).

III. CIRCUIT IMPLEMENTATION

A. FILTERING 180° HYBRID WITH $n = 3$ AND $P_{ratio} = 0$ dB

To verify the design approach, a filtering 180° hybrid with third-order Chebyshev bandpass response (0.04321 dB ripple level) was designed to exhibit a central frequency of 0.52 GHz with a fractional bandwidth of 4.8% and an output power-dividing ratio of 0 dB (equal power division, i.e., $\alpha = \beta = \sqrt{1/2}$). Initially, the net-type resonators were selected to form the filtering 180° hybrid, because this kind of resonator has the properties such as compact size, wide stopband response, and flexible circuit layout [29], [30]. The net-type resonator used in this design was constructed by connecting one short-circuited microstrip line and three identical open-circuited microstrip lines. Here, all microstrip line sections of the net-type resonator were set to the same characteristic impedance. When the resonator operated at the fundamental mode, a maximum electric field density near the open-circuited lines and a maximum magnetic field density near the short-circuited line were observed. Therefore, electric coupling was achieved by closely placing the open-circuited line sections of two net-type resonators, as illustrated in Fig. 6(a), whereas the magnetic coupling was achieved by closely placing the short-circuited line sections of two net-type resonators, as illustrated in Fig. 6(b). Note that, the size of a single net-type resonator is only around $0.06\ \lambda_g \times 0.06\ \lambda_g$, where λ_g is the guided wavelength at the resonance frequency. Moreover, the first harmonic resonance frequency of the net-type resonator occurs at the frequency 5 times above the fundamental resonance frequency, leading to a wide stopband response. In addition, since each stub line of the net-type resonator can be arbitrary bend to form

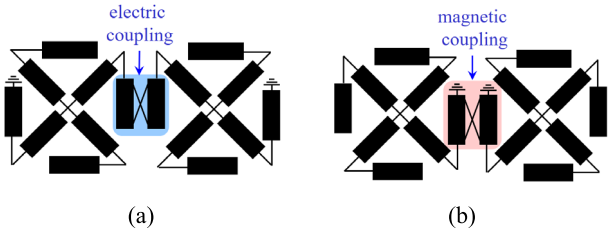

FIGURE 6. Coupling construction of the coupled resonators. (a) Electric coupling and (b) magnetic coupling.

various layouts, thus the property of flexible circuit layout can make it more suitable for implementing the proposed coupling topology of the filtering 180° hybrid.

The coupling topology of the third-order filtering 180° hybrid is displayed in the inset of Fig. 5(a) or (b). The theoretical values of coupling coefficients and external quality factors can be calculated as follows:

$$\begin{aligned} M_{12} = M_{56} &= \frac{\Delta}{\sqrt{g_1 g_2}} = 0.05 \\ M_{23} = M_{24} = M_{35} &= \sqrt{\frac{1}{2}} \cdot \frac{\Delta}{\sqrt{g_2 g_3}} = 0.035 \\ M_{45} &= -\sqrt{\frac{1}{2}} \cdot \frac{\Delta}{\sqrt{g_2 g_3}} = -0.035 \\ Q_e &= \frac{g_1 g_2}{\Delta} = 17.7 \end{aligned} \tag{10}$$

where Δ is the fractional bandwidth; g values are the lumped-element values of a low-pass prototype filter, which are $g_0 = 1, g_1 = 0.8516, g_2 = 1.1032$, and $g_3 = 0.8516$ [26]. The existence of 180° phase difference between the electric and magnetic couplings reveals opposite signs; thus, the positive couplings, M_{12}, M_{56}, M_{23}, M_{24}, and M_{35}, are realized by electric coupling; the negative coupling, M_{45}, is realized by magnetic coupling.

The schematic layout of the filtering 180° hybrid is presented in Fig. 7. The circuit was designed and implemented in microstrip on a 1.524-mm-thick Rogers RO4003 substrate, which exhibited a loss tangent δ of 0.0027 and relative dielectric constant ϵ_r of 3.38. Theoretical values of M_{12}, M_{56}, M_{23}, M_{24}, M_{35}, and M_{45} were used to determine the distances of d_{12}, d_{56}, d_{23}, d_{24}, d_{35}, and d_{45}, respectively; and, the theoretical value of Q_e was used to determine the geometric parameters of the I/O interdigital coupling structure, namely, g, w_1, and l. Notably, the interdigital coupling structure was adopted in this design to enhance the I/O coupling strength and obtain the desired values of Q_e.

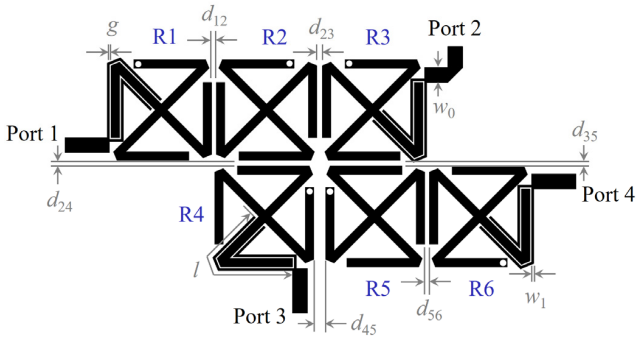

FIGURE 7. Microstrip structure of the third-order filtering 180° hybrid with $P_{ratio} = 0$ dB.

The extracted values of coupling coefficients and external quality factor can be obtained from full-wave simulation results performed by Advanced Design System (ADS). For the extraction of coupling coefficient, the extracted configurations and the simulated frequency responses for electric and magnetic couplings are shown in Fig. 8(a) and (b), respectively. Note that the coupling coefficient could be evaluated using two coupled resonators through the following formula [28]:

$$K = \pm \frac{f_{p2}^2 - f_{p1}^2}{f_{p2}^2 + f_{p1}^2} \tag{11}$$

where f_{p1} and f_{p2} are defined as the lower and higher fundamental resonant frequencies of the two coupled resonators under weak coupling. For the extraction of external quality factor, the extracted configuration and the simulated frequency response are shown in Fig. 9. The external quality factor can be evaluated from an I/O resonator with doubly loading by using the following equation [28]:

$$Q_e = \frac{2f_0}{\Delta f_{3-dB}} \tag{12}$$

where f_0 denotes the resonant frequency and Δf_{3-dB} denotes the 3 dB bandwidth for which $|S_{21}|$ is reduced by 3 dB from its maximum value of the I/O resonator. Following

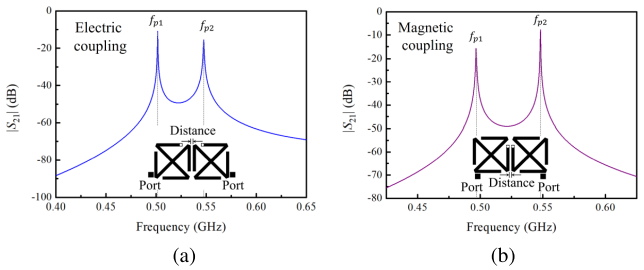

FIGURE 8. Simulated frequency responses of the coupled resonators under weak coupling. (a) Electric and (b) magnetic couplings.

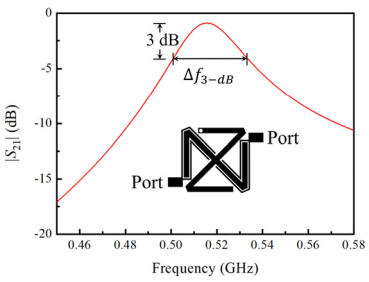

FIGURE 9. Resonant amplitude response of S_{21} for the I/O resonator.

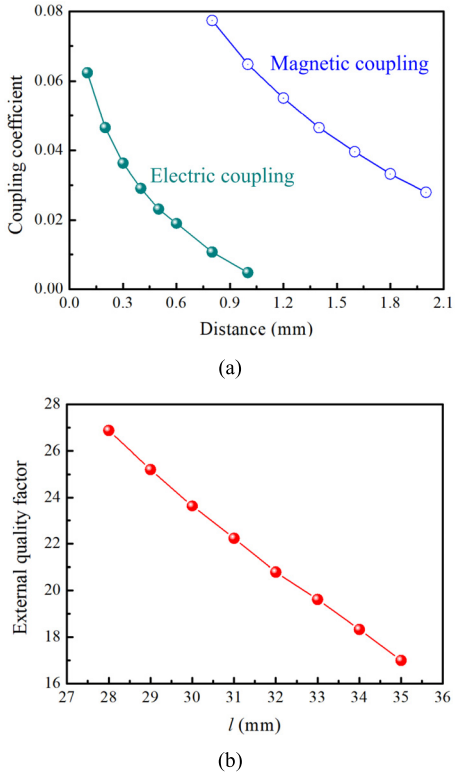

FIGURE 10. Design curves. (a) Extracted coupling coefficient against the gap distance between the adjacent resonators. (b) Extracted external quality factor against l ($w_1 = 0.5$ mm and $g = 0.1$ mm).

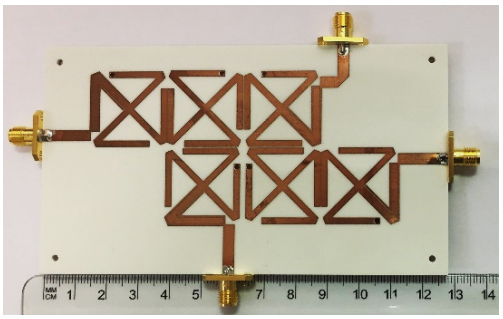

FIGURE 11. Photograph of the fabricated filtering 180° hybrid with $P_{ratio} = 0$ dB.

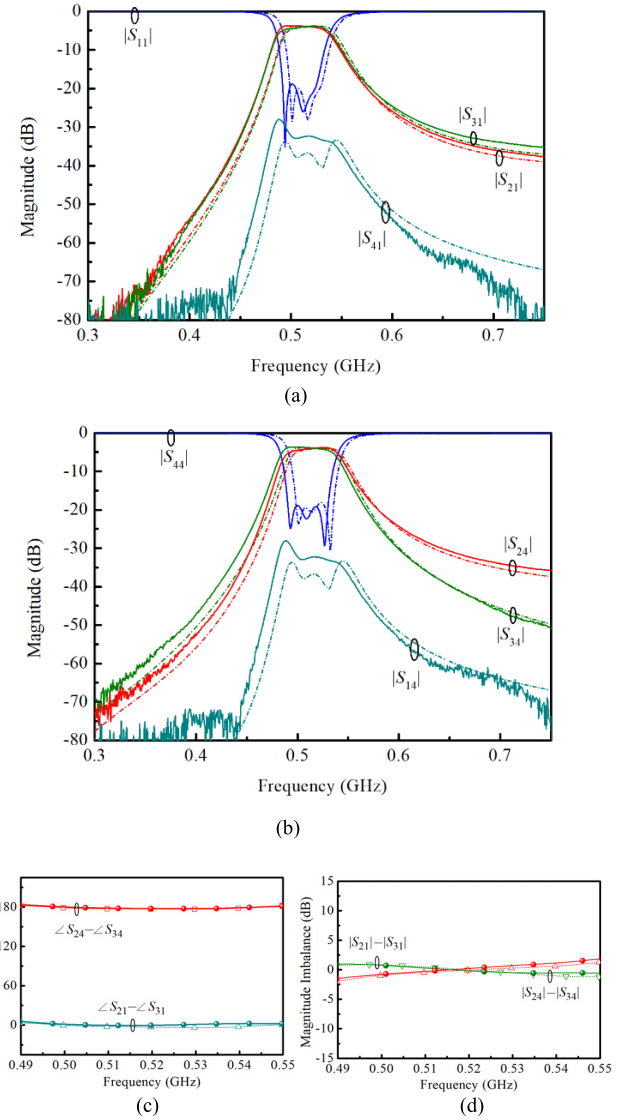

FIGURE 12. Measurement and simulation results of the proposed third-order filtering 180° hybrid with $P_{ratio} = 0$ dB. (a) $|S_{11}|$, $|S_{21}|$, $|S_{31}|$, and $|S_{41}|$; (b) $|S_{44}|$, $|S_{24}|$, $|S_{34}|$, and $|S_{14}|$; (c) phase difference; (d) magnitude imbalance. (Dashed line: simulation results; solid line: measurement results).

the above analysis, the design curves of coupling coefficient and external quality factor can be obtained and plotted in Fig. 10(a) and (b), respectively. After that, the structural parameters of the filtering 180° hybrid can be determined when the extracted values of coupling coefficients and external quality factors correspond to the theoretical values.

The designed third-order filtering 180° hybrid with $P_{ratio} = 0$ dB had an overall circuit area of $0.25\ \lambda_g \times 0.12\ \lambda_g$ (i.e., 97.3×49.7 mm^2), where λ_g was the guided wavelength at the central frequency of the passband (i.e., 0.52 GHz). The structural parameters are listed as follows: $d_{12} = d_{56} = 0.12$ mm, $d_{23} = 0.31$ mm, $d_{24} = d_{35} = 0.36$ mm, $d_{45} = 1.82$ mm, $g = 0.1$ mm, $l = 34.5$ mm, $w_0 = 3.53$ mm, and $w_1 = 0.5$ mm. The photograph of the fabricated filtering 180° hybrid is illustrated in Fig. 11.

Fig. 12(a)–(d) presents the electromagnetic simulation and measurement results of the proposed filtering 180° hybrid. An Agilent N5230A network analyzer was used for measurement. The measurement results were in good agreement with the simulated ones. From the measurement results, the return losses (i.e., $|S_{11}|$ and $|S_{44}|$) were both better than 18 dB within the passband frequencies; and the insertion losses $|S_{21}|$, $|S_{31}|$, $|S_{24}|$, and $|S_{34}|$ at the central frequency were approximately 0.84, 1.1, 1.1, and 0.8 dB, respectively, in addition to the insertion loss of the 3 dB 180° hybrid. Notably, the insertion losses primarily resulted from conductor loss. In addition, the measured isolations (i.e., $|S_{41}|$ and $|S_{14}|$) were both higher

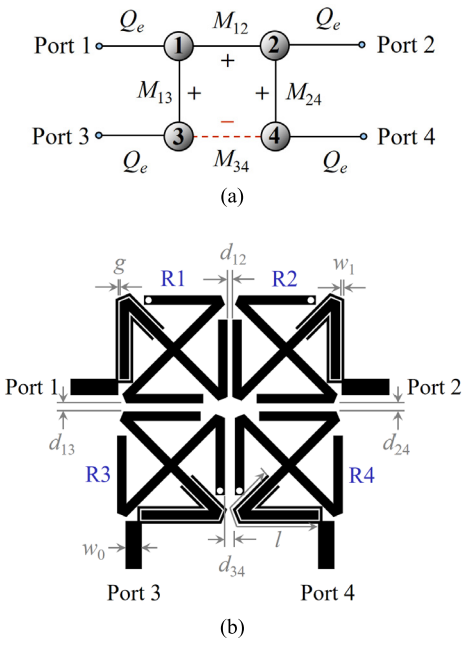

FIGURE 13. Coupling topology and (b) microstrip structure of the second-order filtering 180° hybrid with $P_{ratio} = 6$ dB.

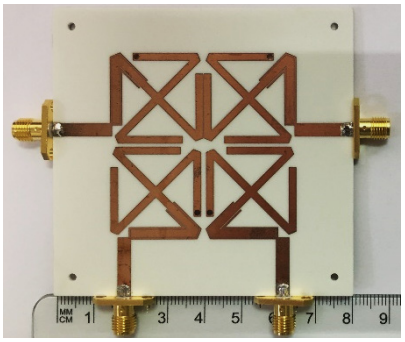

FIGURE 14. Photograph of the fabricated filtering 180° hybrid with $P_{ratio} = 6$ dB.

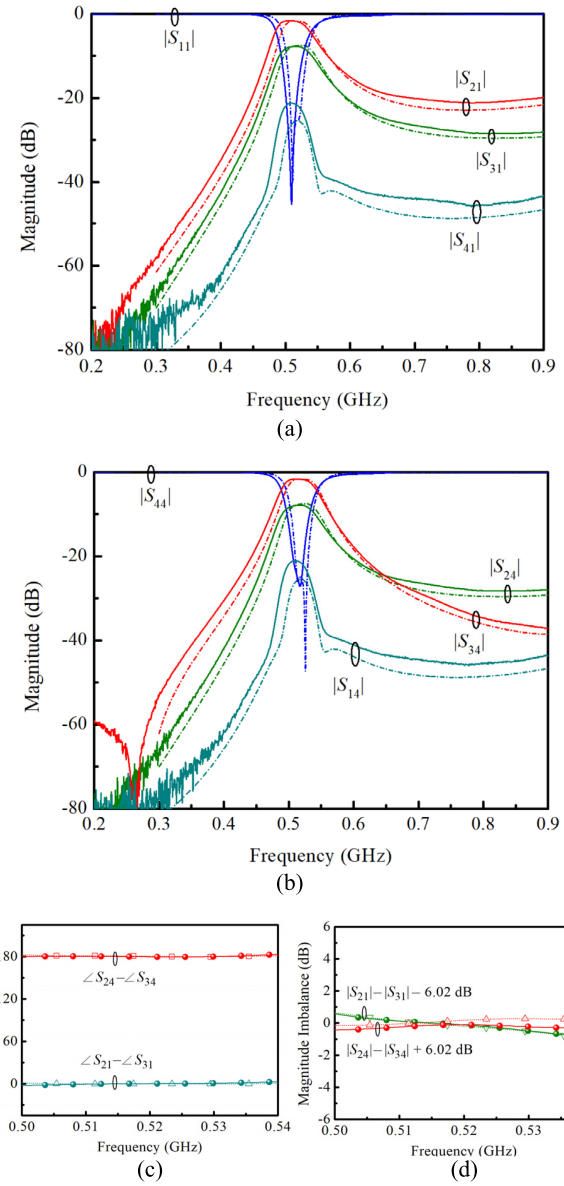

FIGURE 15. Measurement and simulation results of the proposed second-order filtering 180° hybrid with $P_{ratio} = 6$ dB. (a) $|S_{11}|$, $|S_{21}|$, $|S_{31}|$, and $|S_{41}|$; (b) $|S_{44}|$, $|S_{24}|$, $|S_{34}|$, and $|S_{14}|$; (c) phase difference; (d) magnitude imbalance. (Dashed line: simulation results; solid line: measurement results).

than 30 dB over the whole passband. Moreover, the measured phase differences $\angle S_{21}-\angle S_{31}$ and $\angle S_{24}-\angle S_{34}$ ranges from 0.5 to 0.54 GHz were between $-0.89°$ to 1.95° and 178.7° to 180.1°, respectively; the measured magnitude imbalances $|S_{21}| - |S_{31}|$ and $|S_{24}| - |S_{34}|$ from 0.5 to 0.54 GHz were within 0.5 and 0.8 dB, respectively.

B. FILTERING 180° HYBRID WITH n = 2 AND P_{ratio} = 6 dB

In the second design example, a filtering 180° hybrid with second-order Chebyshev bandpass response (0.04321 dB ripple level) was designed to a central frequency of 0.52 GHz with a fractional bandwidth of 3% and an output power-dividing ratio of 6 dB, which indicated that $\alpha = \sqrt{4/5}$ and $\beta = \sqrt{1/5}$. The ideal insertion losses of $|S_{21}|$ and $|S_{31}|$ (or $|S_{34}|$ and $|S_{24}|$) were typically 0.97 and 6.99 dB, respectively. The corresponding coupling topology of the filtering 180° hybrid is shown in the Fig. 13(a). The theoretical values of coupling coefficients and the external quality factor can be computed, respectively, as follows:

$$M_{12} = \sqrt{\frac{4}{5}} \cdot \frac{\Delta}{\sqrt{g_1 g_2}} = 0.045$$
$$M_{13} = M_{24} = \sqrt{\frac{1}{5}} \cdot \frac{\Delta}{\sqrt{g_1 g_2}} = 0.022$$
$$M_{34} = -\sqrt{\frac{4}{5}} \cdot \frac{\Delta}{\sqrt{g_1 g_2}} = -0.045$$
$$Q_e = \frac{g_1 g_2}{\Delta} = 22.16 \tag{13}$$

where $g_0 = 1, g_1 = 0.6648$, and $g_2 = 0.5445$ [26].

TABLE 1. Comparison with other previous circuits.

	Central frequency (GHz)	Insertion losses (dB)	Isolation (dB)	Filtering function	Filter order	Arbitrary power-dividing function	Circuit size (λ_g^2)
This work (case 1)	0.52	0.84	30	Yes	3	Yes	0.03
This work (case 2)	0.52	0.82	21	Yes	2	Yes	0.014
[3]	2	1.33	22	Yes	2	No	0.03
[4]	2.4	0.7	20	Yes	2	No	0.029
[5]	1.5	3	30	Yes	4	No	0.068
[6]	1.5	2.9	25	Yes	3	No	0.044
[7]	1.28	1.86	30	Yes	2	No	0.518
[8]	2.4	1.77	23	Yes	2	No	0.042
[10]	2.4	1.2	34	Yes	2	No	0.18
[11]	2.77, 3.55	2.2, 1.9	20, 12	Yes	2	No	0.168
[12]	1.6, 2.1	2.4, 1.8	27, 24	Yes	2	No	0.073
[13]	2.4	2.2	17	Yes	8	No	0.211
[14]	2.43, 5.82	1, 1.4	23.5, 32.8	Yes	2	No	0.16
[16]	0.88, 1.98	0.2, 0.6	40.3, 29.5	No	N.A.	No	0.125
[17]	2.4, 5.8	3.87, 3.41	18, 15	No	N.A.	No	0.992
[18]	0.9, 1.8	0.5, 0.7	24.4, 33.4	No	N.A.	No	0.011
[19]	7.25, 20.5	1.2, 2	8, 18	No	N.A.	No	N.A.
[22]	2.45, 5.2	0.32, 1.35	22.5, 22.5	No	N.A.	Yes	N.A.
[23]	2.45	0.76	10	No	N.A.	Yes	0.028
[26]	2	0.58	30	Yes	5	Yes	0.773
[30]	1.2	1.4	30	Yes	2	No	0.036

The layout of the filtering 180° hybrid is presented in Fig. 13(b). The net-type resonators were also exploited to form the filtering 180° hybrid. The positive couplings, M_{12}, M_{13}, and M_{24}, were realized using electric coupling; whereas the negative coupling, M_{34}, was realized using magnetic coupling. The circuit was designed and implemented in microstrip on a 1.524-mm-thick Rogers RO4003 substrate, which exhibited a loss tangent δ of 0.0027 and relative dielectric constant ϵ_r of 3.38. The design curves in Fig. 10(a) and (b) can be also applied to this design. The designed second-order filtering 180° hybrid with $P_{ratio} = 6$ dB had an overall circuit area of 0.12 $\lambda_g \times$ 0.12 λ_g (i.e., 48.3 $\times$ 49 mm^2), where λ_g is the guided wavelength at the central frequency of the passband (i.e., 0.52 GHz). The structural parameters are listed as follows: $d_{12} = 0.15$ mm, $d_{13} = d_{24} = 0.53$ mm, $d_{34} = 1.3$ mm, $g = 0.1$ mm, $l = 30.5$ mm, $w_0 = 3.53$ mm, and $w_1 = 0.5$ mm. The photograph of the fabricated filtering 180° hybrid is illustrated in Fig. 14.

Fig. 15(a)–(d) presents the simulation and measurement results of the proposed filtering 180° hybrid. The measurement results were in good agreement with the simulated ones, showing that both filtering and power-dividing functions are achieved simultaneously. The return losses (i.e., $|S_{11}|$ and $|S_{44}|$) were both better than 20 dB within the passband frequencies; and the insertion losses $|S_{21}|$, $|S_{31}|$, $|S_{24}|$, and $|S_{34}|$ at the central frequencies were approximately 0.97 + 0.82, 6.99 + 0.78, 6.99 + 0.87, and 0.97 + 0.75 dB, respectively. Notably, the insertion losses were primarily caused by conductor loss. In addition, the measured isolations (i.e., $|S_{41}|$ and $|S_{14}|$) were both greater than 21 dB over the whole passband. Moreover, the measured phase differences $\angle S_{21} - \angle S_{31}$ and $\angle S_{24} - \angle S_{34}$ ranges from 0.5 to 0.54 GHz were within $0° \pm 3°$ and $180° \pm 3°$, respectively; the measured magnitude imbalances $|S_{21}| - |S_{31}| - 6.02$ dB and $|S_{24}| - |S_{34}| + 6.02$ dB ranges from 0.5 to 0.54 GHz were within 0.8 dB and 0.3 dB, respectively.

Table 1 summarizes the comparison of the proposed filtering 180° hybrids and other reported previous circuits. Both filtering and power-dividing functions were achieved for the proposed 180° hybrids. The frequency selectivity (filter order) and power-dividing ratio can be designed arbitrarily. Moreover, the proposed filtering 180° hybrids occupy small areas. Compared with the design of unequal power division filtering rat-race ring couplers in [26], a smaller circuit area can be obtained by using the proposed method and structure. Depending on the same filter order, operating frequency, and substrate parameters, size reduction greater than 90% can be achievable. In addition, the design in [30] does not provide the

solution for arbitrary power division and arbitrary filtering response (filter order). In other words, the design in [30] is only able to realize a second-order filtering power divider with equal power division.

IV. CONCLUSION

In this paper, the design of filtering 180° hybrids with arbitrary power division and filtering response is proposed. Detailed design theory and steps are provided. Third-order and second-order filtering 180° hybrid with power-dividing ratios of 0 dB and 6 dB, respectively, were designed and implemented to verify the theoretical prediction and design approach. The results demonstrated that both the frequency selectivity (filter order) and power-dividing ratio can be designed arbitrarily. Moreover, the sizes of the two example circuits were only approximately 0.25 $\lambda_g \times$ 0.12 λ_g and 0.12 $\lambda_g \times$ 0.12 λ_g. In addition, in-band isolations higher than 30 and 21 dB were obtained, respectively. As a result, the features of compact size, arbitrary filtering response, arbitrary power division, and high isolation make the proposed filtering 180° hybrids attractive for application in modern RF and microwave systems.

REFERENCES

[1] D. M. Pozar, *Microwave Engineering*, 2nd ed. New York, NY, USA: Wiley, 1998.

[2] H. Uchida, N. Yoneda, Y. Konishi, and S. Makino, "Bandpass directional couplers with electromagnetically-coupled resonators," in *IEEE MTT-S Int. Microw. Symp. Dig., San Francisco, CA, Jun.*, Jun. 2006, pp. 1563–1566.

[3] W.-H. Wang, T.-M. Shen, T.-Y. Huang, and R.-B. Wu, "Miniaturized rat-race coupler with bandpass response and good stopband rejection," in *IEEE MTT-S Int. Microw. Symp. Dig.*, Boston, MA, USA, Jun. 2006, pp. 1563–1566.

[4] C.-K. Lin and S.-J. Chung, "A compact filtering 180° hybrid," *IEEE Trans. Microw. Theory Techn.*, vol. 59, no. 12, pp. 3030–3036, Dec. 2011.

[5] C.-F. Chen, T.-Y. Huang, C.-C. Chen, W.-R. Liu, T.-M. Shen, and R.-B. Wu, "A compact filtering rat-race coupler using dual-mode stub-loaded resonators," in *IEEE MTT-S Int. Microw. Symp. Dig.*, Montreal, QC, Canada, Jun. 2012, pp. 1–3.

[6] W.-R. Liu, T.-Y. Huang, C.-F. Chen, T.-M. Shen, and R.-B. Wu, "Design of a 180-degree hybrid with Chebyshev filtering response using coupled resonators," in *IEEE MTT-S Int. Microw. Symp. Dig.*, Seattle, WA, USA, Jun. 2013, pp. 1–3.

[7] Y.-L. Lu, Y. Wang, C. Hua, and T. Liu, "Design of compact filtering rat-race hybrid with λ/2-resonators," *Electron. Lett.*, vol. 52, no. 21, pp. 1780–1782, Oct. 2016.

[8] T.-W. Lin, J.-Y. Wu, and J.-T. Kuo, "Filtering rat-race coupler with transmission zeros using compact miniaturized hairpin resonators," in *Proc. IEEE Int. Wireless Symp.*, Shenzhen, China, Mar./Apr. 2015, pp. 1–4.

[9] V. T. di Crestvolant, P. M. Iglesias, and M. J. Lancaster, "Advanced butler matrices with integrated bandpass filter functions," *IEEE Trans. Microw. Theory Techn.*, vol. 63, no. 10, pp. 3433–3444, Oct. 2015.

[10] Q. Shao, F.-C. Chen, Q.-X. Chu, and M. J. Lancaster, "Novel filtering 180° hybrid coupler and its application to 2×4 filtering butler matrix," *IEEE Trans. Microw. Theory Techn.*, vol. 66, no. 7, pp. 3288–3296, Jul. 2018.

[11] F. Lin, Q.-X. Chu, and S. W. Wong, "Design of dual-band filtering quadrature coupler using λ/2 and λ/4 resonators," *IEEE Microw. Wireless Compon. Lett.*, vol. 22, no. 11, pp. 565–567, Nov. 2012.

[12] C.-F. Chen, S.-F. Chang, and B.-H. Tseng, "Compact microstrip dual-band quadrature coupler based on coupled-resonator technique," *IEEE Microw. Wireless Compon. Lett.*, vol. 26, no. 7, pp. 487–489, Jul. 2016.

[13] C.-H. Lin and J.-T. Kuo, "Compact eighth-order microstrip filtering coupler," in *Proc. IEEE Asia Pacific Microw. Conf. (APMC)*, Kuala Lumpar, Malaysia, Nov. 2017, pp. 806–808.

[14] L.-S. Wu, B. Xia, W.-Y. Yin, and J. Mao, "Collaborative design of a new dual-bandpass 180° hybrid coupler," *IEEE Trans. Microw. Theory Techn.*, vol. 61, no. 3, pp. 1053–1066, Mar. 2013.

[15] I.-H. Lin, M. DeVincentis, C. Caloz, and T. Itoh, "Arbitrary dual-band components using composite right/left-handed transmission lines," *IEEE Trans. Microw. Theory Techn.*, vol. 52, no. 4, pp. 1142–1149, Apr. 2004.

[16] K.-K. M. Cheng and F.-L. Wong, "A novel rat race coupler design for dual-band applications," *IEEE Microw. Wireless Compon. Lett.*, vol. 15, no. 8, pp. 521–523, Aug. 2005.

[17] K.-S. Chin, K.-M. Lin, Y.-H. Wei, T.-H. Tseng, and Y.-J. Yang, "Compact dual-band branch-line and rat-race couplers with stepped-impedance-stub lines," *IEEE Trans. Microw. Theory Techn.*, vol. 58, no. 5, pp. 1213–1221, May 2010.

[18] G.-Q. Liu, L.-S. Wu, and W.-Y. Yin, "Miniaturised dual-band rat-race coupler based on double-sided parallel stripline," *Electron. Lett.*, vol. 47, no. 14, pp. 800–802, Jul. 2011.

[19] T. Djerafi, H. Aubert, and K. Wu, "Ridge substrate integrated waveguide (RSIW) dual-band hybrid ring coupler," *IEEE Microw. Wireless Compon. Lett.*, vol. 22, no. 2, pp. 70–72, Feb. 2012.

[20] Y.-C. Chiou, J.-S. Wu, and J.-T. Kuo, "Periodic stepped-impedance rat race coupler with arbitrary power division," in *Proc. Asia–Pacific Microw. Conf.*, Yokohama, Japan, Dec. 2006, pp. 663–666.

[21] C.-Y. Wu, Y.-C. Chiou, and J.-T. Kuo, "Dual-band rat-race coupler with arbitrary power divisions using microwave C-sections," in *Proc. Asia Pacific Microw. Conf.*, Singapore, Dec. 2009, pp. 2108–2111.

[22] C.-L. Hsu, J.-T. Kuo, and C.-W. Chang, "Miniaturized dual-band hybrid couplers with arbitrary power division ratios," *IEEE Trans. Microw. Theory Techn.*, vol. 57, no. 1, pp. 149–156, Jan. 2009.

[23] C.-H. Lu, P.-H. Tu, and C.-H. Tseng, "A miniaturized rat-race coupler with arbitrary power division using dual transmission lines," in *Proc. Asia Pacific Microw. Conf.*, Kaohsiung, Taiwan, Dec. 2012, pp. 1007–1009.

[24] L.-S. Wu, J. Mao, and W.-Y. Yin, "Miniaturization of rat-race coupler with dual-band arbitrary power divisions based on stepped-impedance double-sided parallel-strip line," *IEEE Trans. Compon., Packag., Manuf. Technol.*, vol. 2, no. 12, pp. 2017–2030, Dec. 2012.

[25] G. Chaudhary and Y. Jeong, "Arbitrary power division ratio rat-race coupler with negative group delay characteristics," *IEEE Microw. Wireless Compon. Lett.*, vol. 26, no. 8, pp. 565–567, Aug. 2016.

[26] P.-J. Chou, C.-C. Yang, and C.-Y. Chang, "Exact synthesis of unequal power division filtering rat-race ring couplers," *IEEE Trans. Microw. Theory Techn.*, vol. 66, no. 7, pp. 3277–3287, Jul. 2018.

[27] K. S. Ang and Y. C. Leong, "Converting baluns into broad-band impedance-transforming 180° hybrids," *IEEE Trans. Microw. Theory Techn.*, vol. 50, no. 8, pp. 1990–1995, Aug. 2002.

[28] J.-S. G. Hong and M. J. Lancaster, *Microstrip Filters for RF / Microwave Applications*. New York, NY, USA: Wiley, 2001.

[29] C.-F. Chen, T.-Y. Huang, and R.-B. Wu, "Novel compact net-type resonators and their applications to microstrip bandpass filters," *IEEE Trans. Microw. Theory Techn.*, vol. 54, no. 2, pp. 755–762, Feb. 2006.

[30] C.-F. Chen and C.-Y. Lin, "Compact microstrip filtering power dividers with good in-band isolation performance," *IEEE Microw. Wireless Compon. Lett.*, vol. 24, no. 1, pp. 17–19, Jan. 2014.

CHI-FENG CHEN (M'12) was born in Pingtung, Taiwan, in 1979. He received the M.S. degree in electrophysics from National Chiao Tung University, Hsinchu, Taiwan, in 2003, and the Ph.D. degree in communication engineering from National Taiwan University, Taipei, Taiwan, in 2006.

From 2008 to 2010, he was a Radio-Frequency (RF) Engineer with Compal Communications, Inc., Taipei, Taiwan, where he developed global system for mobile communication and code-division multiple access mobile phones. In 2010, he joined the Graduate Institute of Communication Engineering, National Taiwan University, as a Post-doctoral Research Fellow. Since 2012, he has been with the Department of Electrical Engineering, Tunghai University, Taichung, Taiwan, as an Assistant Professor, where he became an Associate Professor, in 2016. His research interests include the design of microwave circuits and associated RF modules for microwave and millimeter-wave applications.

JHONG-JHEN LI was born in Changhua, Taiwan, in 1988. He received the B.S. and M.S. degrees in electrical engineering from Tunghai University, Taichung, Taiwan, in 2010 and 2019, respectively. His current research interest includes the design of microwave circuits.

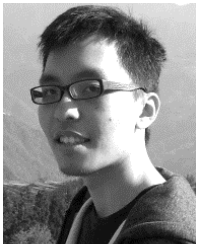

GUO-YUN WANG was born in Taichung, Taiwan, in 1994. He received the B.S. and M.S. degrees in electrical engineering from Tunghai University, Taichung, Taiwan, in 2016 and 2018, respectively. His current research interest includes the design of microwave circuits.

KAI-WEI ZHOU was born in Keelung, Taiwan, in 1996. He is currently pursuing the M.S. degree with the Department of Electrical Engineering, Tunghai University, Taichung, Taiwan. His current research interests include the design of microwave circuits.

RUEI-YI CHEN was born in Kaohsiung, Taiwan, in 1997. She is currently pursuing the M.S. degree with the Department of Electrical Engineering, Tunghai University, Taichung, Taiwan. Her current research interest includes the design of microwave circuits.